

Article

A Bi-State Shape Memory Material Composite Soft Actuator

Ramprasad Rajagopalan ^{1,2} , Andrew J. Petruska ²  and David Howard ^{1,*} 

¹ Robotics and Autonomous Systems Group, Data61, CSIRO, Brisbane 4069, Australia; ramprasad.raj28@gmail.com

² Mechanical Engineering and Robotics, Colorado School of Mines, Golden, CO 80401, USA; apetruska@mines.edu

* Correspondence: david.howard@csiro.au

Abstract: Shape memory materials have been widely used as programmable soft matter for developing multifunctional hybrid actuators. Several challenges of fabrication and effective modelling of these soft actuating systems can be addressed by implementing novel 3D printing techniques and simulations to aid the designer. In this study, the temperature-dependent recovery of an embedded U-shaped Shape Memory Alloy (SMA) and the shape fixity of a 3D-printed Shape Memory Polymer (SMP) matrix were exploited to create a bi-state Shape Memory Composite (SMC) soft actuator. Electrical heating allowed the SMA to achieve the bi-state condition, undergoing phase transformation to a U shape in the rubbery phase and a flat shape in the glassy phase of the SMP. A COMSOL Multiphysics model was developed to predict the deformation and recovery of the SMC by leveraging the in-built SMA constitutive relations and user-defined material subroutine for the SMP. The bi-state actuation model was validated by capturing the mid-point displacement of the 80 mm length × 10 mm width × 2 mm-thick 3D-printed SMC. The viability of the SMC as a periodic actuator in terms of shape recovery was addressed through modelling and simulation. Results indicated that the proposed COMSOL model was in good agreement with the experiment. In addition, the effect of varying the volume ratio of the SMA wire in the SMC on the maximum and recovered deflection was also obtained. Our model can be used to design SMC actuators with various performance profiles to facilitate future designs in soft robotics and wearable technology applications.

Keywords: soft actuators; soft robotics; shape memory material; shape memory alloy; shape memory polymer; composite actuator; multi-physics modelling



Citation: Rajagopalan, R.; Petruska, A.J.; Howard, D. A Bi-State Shape Memory Material Composite Soft Actuator. *Actuators* **2022**, *11*, 86. <https://doi.org/10.3390/act11030086>

Academic Editor: Wei Min Huang

Received: 13 January 2022

Accepted: 7 March 2022

Published: 11 March 2022

Publisher's Note: MDPI stays neutral with regard to jurisdictional claims in published maps and institutional affiliations.



Copyright: © 2022 by the authors. Licensee MDPI, Basel, Switzerland. This article is an open access article distributed under the terms and conditions of the Creative Commons Attribution (CC BY) license (<https://creativecommons.org/licenses/by/4.0/>).

1. Introduction

Smart materials responding to an external stimuli can be used to fabricate smart actuators for applications ranging from wearable technology to self-folding aerospace structures [1–3]. Extensive research in robotics has been carried out to utilise such devices to address the common challenges faced by rigid robots such as adaptable locomotion within a complex environment and safe interaction with human beings [4]. The emergence of soft robotics at the intersection of smart materials, advanced fabrication techniques, and computational design addresses these challenges by drawing inspiration from biological organisms [5]. The structural design of biological organisms is composed of soft and hard materials, with associated synchronised neuromechanical control. In order to develop robots mimicking such organisms, flexible actuation to deliver continuous deformation and embodiment of stiffness modulation through environmental interaction are essential [6]. The advent of additive manufacturing technologies, progress in material science, and advances in soft material simulation software support the design and fabrication of such complex metamaterial soft actuation structures.

Various smart actuators including pneumatic, magnetic, light-induced liquid crystalline elastomers, dielectric elastomers, SMPs, and SMAs have been developed to be entirely soft and provide compliant actuation [4,7]. Shape memory materials, including

SMA and SMPs, belong to the class of smart materials that can be programmed to memorise a geometric shape and possess the ability to recover that shape from large deformation by external stimuli. Extensive studies have been implemented on thermal or electro-active shape memory materials in their usage as an actuator for deformable structures [8–10]. In this work, a composite actuator was fabricated using the SMP and SMA to achieve bending actuation by electrical heating methods. Four-dimensional printing technology was utilised in this study to provide the shape memory effect in the SMP. The SMA and SMP were considered as 4D materials for actuators utilising electrical actuation in the next phase of the 3D printing model [11]. The strength-to-weight ratio of the SMA and stiffness modulation properties of the SMP were extensively exploited to fabricate smart actuators. However, the SMA was limited by a smaller actuation strain with a complex shape memory effect caused due to stress in addition to temperature, and the SMP possessed low recovery stress and conductivity in addition to a higher cost.

Recent studies have implemented composite structures by utilising the complementary behaviour of SMAs and SMPs [9,12]. Composites with a higher recovery force and stiffness modulation in the structure can be achieved in a small form factor by combining SMAs and SMPs. By having complementary stiffness behaviours between SMAs and SMPs, periodic actuators can be devised by having the SMP as the energy storing element and the SMA as the high energy density actuator. In comparison to other actuators, this union can be programmed to different configurations and employ fewer drive elements, and an array of them can form multimodal robots. A curved actuator having a 3D-printed SMP matrix with Nylon-12-based SMP filaments was embedded with electrically heated SMA wires having a memorised straight shape. Kang et al. [11] demonstrated the bi-state actuation of this composite for valve application by analysing the effect of the volume fraction of the SMA and SMP. Researchers have proposed a thermomechanical constitutive model to predict the bending of an actuator with linearly actuating SMA wire in between resin-based SMP layers [13]. The model was further validated, and the parameters were obtained by performing thermo-mechanical experiments. Another study demonstrated the application of shape memory composites in smart valves and tents by reinforcing straight SMA wires in a resin-based SMP matrix. Most of the studies performed designed the optimisation and estimation of the model parameters based on trial and error. In order to efficiently utilise the resources along with a reduction of the time, the design can be optimised by focusing on computational methods. Manzo et al. [8] proposed an analytical and ANSYS model for a multi-layer smart joint with a linearly actuating SMA over an SMP layer. The model was utilised in proposing a joint for wing morphing and biological flight structures. A Fortran-run material sub-routine in the Abaqus simulation aided the design of the shape memory composite laminate to maximise the deflection under the given constraints [14]. The model was intended to demonstrate its application in developing a locking mechanism and self-assembling structures. A rapid solar sail deployment mechanism was achieved by having electrically driven SMA wires. Mathematical models demonstrating the actuation mechanism were implemented for various configurations and compared with the experimental studies for deployment time and folds [15]. A few earlier works fabricated multi-state SMC from epoxy resins and prestrained SMA wires [16,17]. Although these studies employed analytical modelling or experimental validation to demonstrate the applicability of the design, the high cost involved in the fabrication procedures and complicated numerical models restricted the usability for complex designs. The computational models were limited by time complexity and modelling the multiphysics as an overhead.

Based on the literature, apart from linear actuation for SMAs, there exists a gap in the research for analysing different morphologies of the shape memory effect. The SMA with a pre-curved memorised geometry was used in this study to obtain larger deformation with smaller bending strain. Four-dimensional printing fabrication techniques were explored to program the flat memorised shape in the SMP matrix. COMSOL Multiphysics simulation, Version 5.5 [18], was utilised with an in-built material model for the SMA and an external C subroutine for the SMP to model the complex interactions. A generic workflow to devise

such shape memory actuators in future designs and analysing the viability for periodic actuation was proposed in this study. The proposed model was validated by conducting the required experiments, and the number of parameters was restricted by only obtaining the properties, which largely affected the behaviour of the model. The study identified that the transition temperatures played an important role in the shape recovery and energy requirements of the composites. The proposed model can prevent unwanted consumption of materials and speed up the fabrication process thorough the design.

The paper is structured as follows. Section 2 discusses the actuation mechanism of the SMC by describing the theoretical actuation of the SMA and SMP; Section 2.1 explains the fabrication and material characterisation process of the SMC; Section 2.2 discusses the COMSOL Multiphysics simulation of the SMC to obtain the deflection of the actuator with respect to temperature; Section 3 validates the results of periodic actuation model (in COMSOL Multiphysics) with the results from physical actuation of the SMC; Section 4 provides conclusive evidence that the proposed FEA model describes the behaviour of the SMC.

2. Materials and Methods

The theoretical actuation of the SMA provided here was based on the concepts from Lagoudas [19]. The theoretical actuation of the SMP provided here was based on the concept presented in Hu et al. [20]. In this study, the mechanical programming of the SMP was implemented by the FDM technique to fabricate flat memorised structures with minimum prestrain to exploit the shape memory behaviour of the SMP.

The design and fabrication of the SMC for periodic actuation was governed by the location of the transformation temperatures of the SMA and SMP. This study programmed the SMC to have the glass transition temperature of the SMP, T_g , to be less than the martensite finish temperature of the SMA, M_f , in order to possess the bi-state condition with a single one-way actuating SMA and SMP.

As can be seen from Figure 1, the T_g of the SMP should be as low as possible relative to the M_f of the SMA for the desired behaviour to occur. Nevertheless, it should not be close to room temperature as the SMP loses the rigidity offered to the otherwise soft SMA in the structure. Apart from the transformation temperatures, the flexural stiffness and adhesion between the SMA and SMP play a critical role for the desired behaviour. The proposed actuation mechanism was based on the work presented by Taya et al. [16]. The periodic two-way actuation of the SMC was realised by exploiting the viscoelastic nature of the SMP to store and dissipate strain energy and the memorised shape of both the SMA and SMP. Figure 2 depicts the periodic working mechanism of the SMC due to the phase transformation and relative stiffness. The SMA had a memorised U shape, and the SMP had a memorised flat shape. The U-shaped SMA was prestrained by making it flat and placed in the SMC. At room temperature, as the SMP was in the memorised flat shape, the SMC remained flat. As the temperature was increased, the SMP transformed to the rubbery phase and became soft. When the temperature of the SMC reached the austenite start temperature of the SMA, A_s , it underwent a phase transformation from martensite to austenite and started to recover its memorised U shape. This induced strain in the SMP, and the strain energy was stored during the entire SMA transformation. When the SMC started to cool, the rubbery phase SMP released the stored strain energy and worked against the stiffness of the austenitic SMA. When the temperature of the SMC was greater than the martensite start temperature of the SMA, M_s , the geometry remained the same as the soft SMP could not overcome the stiffness of the austenitic SMA. Upon further cooling to the martensite finish temperature of the SMA, M_f , the SMA transformed to martensite, thereby becoming soft. The antagonistic SMP could now work against the stiffness of the SMA in order to recover its memorised flat shape. The shape recovery occurred only till the rubbery phase became transformed to the glassy phase when the temperature fell below T_g . The process was repeated again to achieve periodic actuation by exploiting the shape recovery of the stiff SMA and storing the elastic energy in the rubbery SMP. The design of such an

SMC was effective as the complementary behaviour of the SMA and SMP circumvented the presence of external biasing elements.

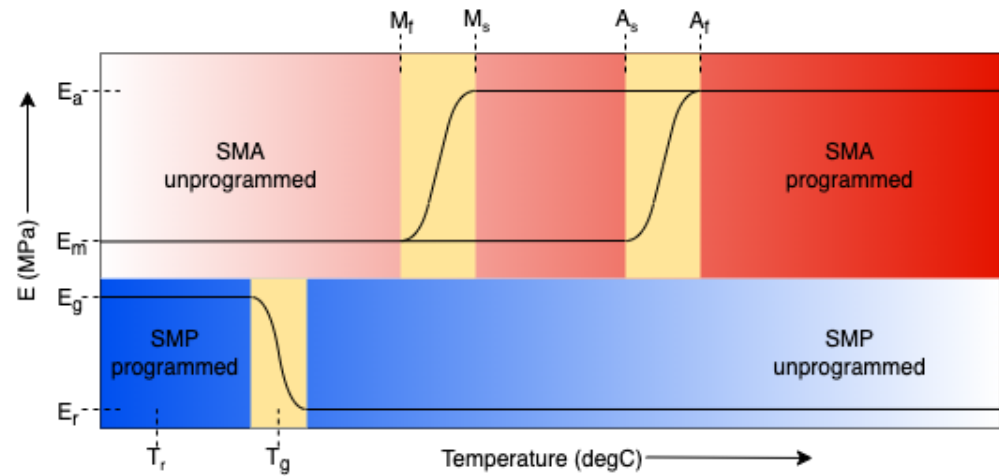


Figure 1. Complementary behaviour of the SMA and SMP dictating the periodic actuation obtained from the variation in stiffness with respect to temperatures (not to scale). Based on [19].

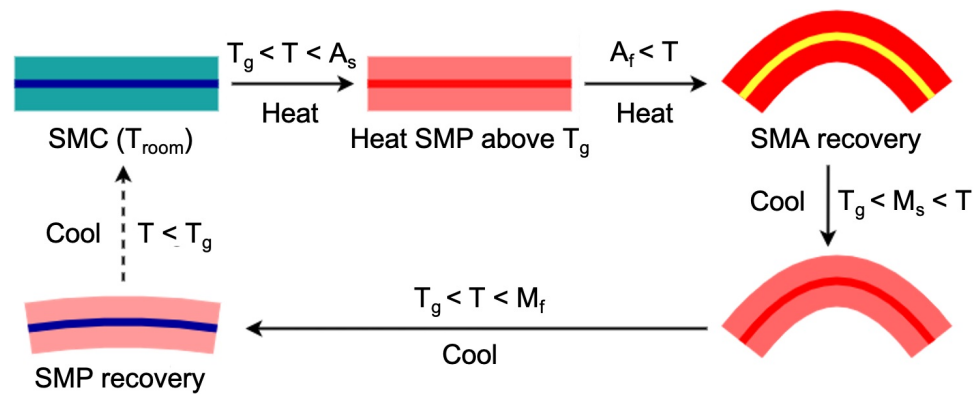


Figure 2. Schematic diagram of periodic actuation of the SMC obtained by undergoing a sequence of phase transformations due to temperature variation and the relative stiffness of the SMA and SMP.

2.1. Fabrication and Material Characterisation

The fabrication of the SMC using additive manufacturing techniques and physical metallurgical process is explained in this section. In order to simulate and validate the FEA model, certain intrinsic parameters of the SMC needed to be determined. The following section provides a detailed explanation of the characterisation procedure of the SMC.

2.1.1. Sample Preparation

The popular choice of off-the-shelf SMA has a material constitution of Cu-Al-Ni or NiTi and possesses geometries such as wires, ribbon, pipes, foils, etc. A NiTi-based SMA ribbon, 1 mm thick and 5 mm wide, Fort Wayne Metals, and an SMA wire, 0.31 mm in diameter, Dynalloy Inc., was used in this study. The as-received SMA was cut into two pieces of the desired length to shape-set the curvature using heat treatment techniques. One of the heat-treated specimens cut to the desired length was used for determining the transformation temperatures from Differential Scanning Calorimetry (DSC). The other specimen was utilised for fabricating the SMC.

A polyurethane-based SMP 3D filament of 1.75 mm diameter, SMP Technologies Inc., was used in this study for rapid prototyping. The FDM printer, Cetus MK3 Extended by Tiertime Technology with a build volume of 180 mm × 180 mm × 280 mm, was

employed to fabricate the specimen. The printer was set with a 0.4 mm-diameter nozzle having an extrusion temperature of 210 °C and a scanning speed of 20 mm/s with a 40 °C bed temperature. As the behaviour of the 3D-printed specimen was sensitive to raster orientation and possessed anisotropy [20], the raster orientation was chosen by using the slicer, SciSlice, to be either along the longitudinal or transverse direction with a layer height of 0.3 mm. The phase transition behaviour and viscoelastic nature of the SMP were obtained by performing Dynamic Mechanical Analysis (DMA). The test was performed on three beam-like samples having average dimensions of 10 mm length \times 2.98 mm width \times 1.42 mm thick with 5 layers of 100% infill and the raster orientation along the longitudinal direction. In order to characterise the mechanical elastic properties of the 3D-printed SMP such as Young's modulus E and Poisson's ratio ν , uniaxial tensile tests were performed according to the ASTM D638 Type I [21] standard's geometry and sample dimensions. Four dog-bone specimens having twenty-three layers of 100% infill with liquefier movement along the gauge direction were fabricated, and arithmetic mean values from them were recorded.

2.1.2. Shape Setting and Characterisation of the SMA

Most of the commercially available SMA actuators are pretrained to memorise a particular geometry. The parent phase of such actuators can be reprogrammed by the process of shape setting. In order to program the required curvature of the SMA ribbon or wire in the parent phase, heat treatment was performed. This process influences the transformation temperatures of the alloy and effective memorised curvature. The as-received alloy ribbon was initially at super-elastic austenite phase and had a memorised flat shape at room temperature. The as-received alloy wire was in the martensite state with a memorised straight shape at A_f of 70 °C. The following steps illustrate the shape setting process of the alloy ribbon, and similar steps were executed for shape setting the alloy wire. First, the alloy was heat treated at 480 °C for 12 h to release any residual stress and quenched immediately to achieve the soft martensite phase at room temperature. The previous step was performed for the reproducibility of the experiment, but it is not strictly necessary. After that, it was set to the required curvature with the help of a metal fixture. Finally, the setup was placed in a furnace at 510 °C for about 10 min and immediately quenched. This reoriented the crystal structure and programmed the required curvature at the parent austenite phase. The latter step was repeated at least 6 to 8 times to uniformly shape-set the alloy. The shape setting procedure of the SMA altered the zero-stress phase transformation temperatures. The phase transformation temperatures of the shape-set NiTi SMA specimen were obtained from DSC. The prepared sample was kept inside a crucible in the form of wires and analysed for temperatures between -35 °C and 200 °C at a rate of 10 °C/min using the DSC instrument (Mettler Toledo DSC3). The plots from the DSC testing, shown in Figure 3, provide the phase transformation temperatures obtained during heating and cooling. Here, A_s was obtained as 56.99 °C, A_f as 74.48 °C during heating, M_s as 66.42 °C, and M_f as 45.67 °C. Due to a limitation on the testing capability, properties such as thermal conductivity, resistivity, and stress gradient with respect to temperature were obtained from the literature [22].

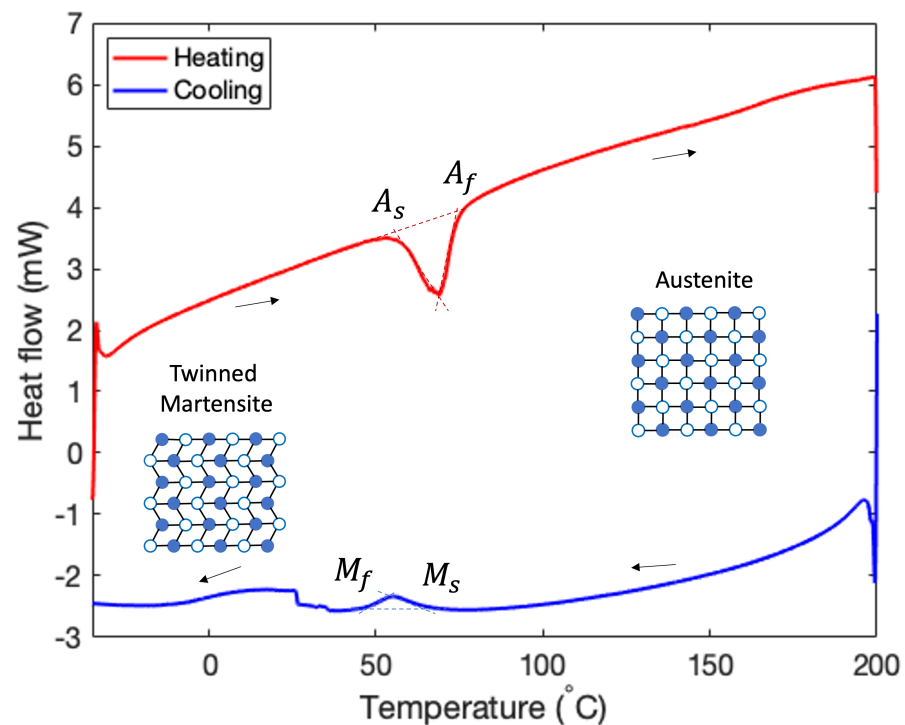


Figure 3. The DSC of the NiTi SMA wire depicts the transformation temperatures by intersecting tangents to the peak, A_s at 56.99 °C, A_f at 74.48 °C during the heating cycle (coloured blue), and M_s at 66.42 °C, M_f at 45.67 °C during the cooling cycle (coloured red).

2.1.3. Characterisation of SMP

The DMA was performed using the DM analyser (Mettler Toledo TT-DMA). The test was setup with a 1 Hz frequency of force oscillation, and the sample was heated at a rate of 2 °C/min from 25 °C to 120 °C. The temperature-dependent viscoelastic properties, such as the storage modulus (E') and phase lag ($\tan \delta$), obtained from the DMA test are shown in Figure 4. E' provides the elastic energy response of the material, and $\tan \delta$ indicates the ratio between the energy dissipated as heat and the energy stored elastically. As can be seen from Figure 4, the storage modulus drastically reduced from 158 MPa in the glassy phase to roughly two orders of magnitude less at 0.3 MPa in the rubbery phase. The maximizing temperature of the $\tan \delta$ function represents the glass transition temperature T_g of the SMP, which in this case was attained at 46.83 °C. The mean value of all three DMA specimen was obtained as 44.59 °C, and this value was considered for modelling purposes. The tensile tests were executed on an MTS 9 Landmark (MTS Testing Solution) fit with a 250 kN load cell and mobile heating chamber. Three samples each were utilised for performing the test at room temperature and a high temperature of 70 °C. The average material properties obtained from the tests are reported in Table 1. It can be seen that the Young's modulus of the SMP in the rubbery phase increased by three orders of magnitude upon transformation to the glassy phase. Further, the Poisson's ratio of the SMP increased from 0.41 in the glassy phase to 0.48 in the rubbery phase, displaying the increase in the incompressibility of the SMP. Due to a limitation on the testing capability, the thermal transport properties, such as the thermal conductivity and specific heat capacity at constant pressure, required for the COMSOL model were obtained from the literature [14].

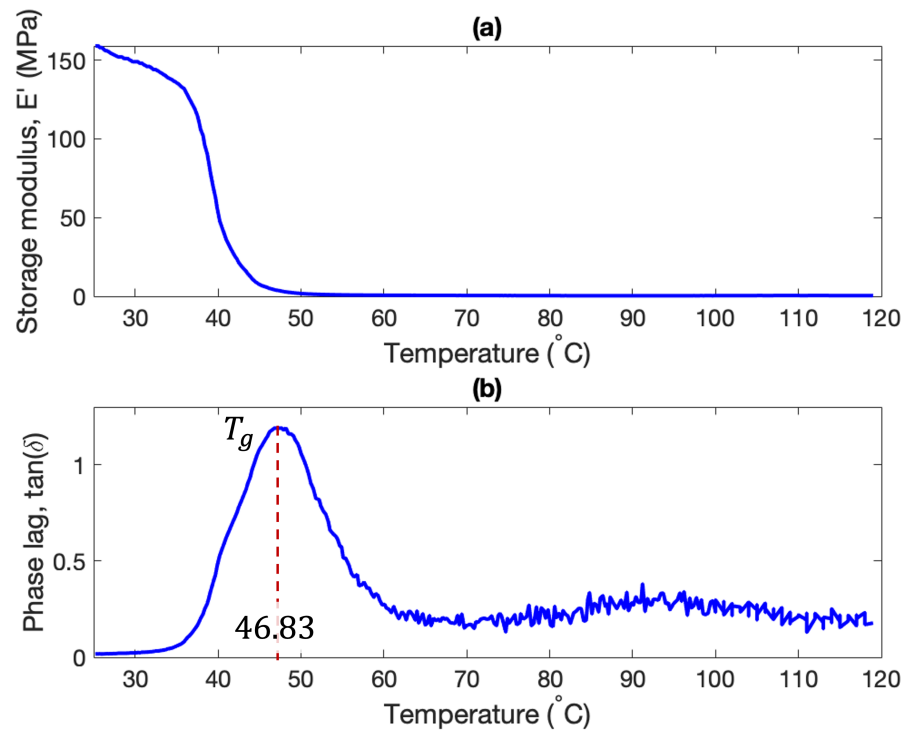


Figure 4. SMP viscoelastic properties and phase transition behaviour from the DMA test: (a) storage modulus; (b) phase lag, $\tan \delta$. The glass transition temperature, T_g at 46.83 °C, is the peak of the phase lag curve (shown by the red dashed line) for this particular specimen.

Table 1. Average Young's modulus and Poisson's ratio of the 3D-printed SMP.

Property	Glassy Phase	Rubbery Phase
Poisson's ratio, ν	0.41	0.48
Young's Modulus, E	1668.1 (MPa)	1.64715 (MPa)

2.1.4. Fabrication of the SMC

In this study, the SMC was fabricated to test and validate the model of periodic actuation by having a U-shape-set SMA in an SMP matrix. Figure 5 depicts the process of fabricating the SMC. First, the SMA was prestrained to a straight shape using a mandrel or wire straightener. Care must be employed while prestraining, as it affected the recovery behaviour of the SMA. The SMP matrix was laid flat along the length and cut horizontally to generate the tool path by having a 0.3 mm layer thickness, a nozzle temperature of 210 °C, and a printing speed of 20 mm/s. In order to place the prestrained SMA wire, the middle layer was modified to have a groove along the length with the width equal to the diameter of the wire. The generated G-code had the provision to stop in between the print in order to place the wire. The prestrained SMA wire was placed and ensured to be flush with the printed surface. The print was then resumed to finish the rest of the SMP layers. In order to test the concept of the actuation mechanism and validate the COMSOL Multiphysics model, a sample of 80 mm length \times 10 mm width \times 1.2 mm thick was fabricated using this 3D printing setup.

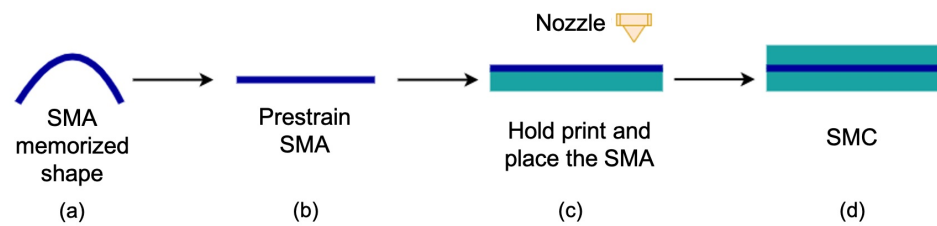


Figure 5. Schematic fabrication process of the SMC: prestrain the SMA wire from its memorised U shape using a mandrel or straightener (a,b); 3D print the SMP layers until the layer with grooves for placing the prestrained SMA (c); 3D print the rest of the SMP layers (d).

Figure 6 shows the labelled picture of the fabricated SMC along with the connecting wire. The U-shaped SMA wire was prestrained to a straight shape and placed inside the SMP matrix. The ends of the SMA wire were crimped to connect to the power source (Dr.Meter PS-3010DF). The deflection was captured using the Pointgrey Grasshopper machine vision camera, and the temperature was monitored using the Optris PI450 infrared camera. The fabricated SMC was placed on the ground, and a constant output current of 2.2 A was provided by the power supply to heat the SMA using Joule heating to above the A_f temperature. The power supply was then turned off to decrease the temperature of the SMC. The deflection data with respect to time were obtained using the snapshots from the camera.

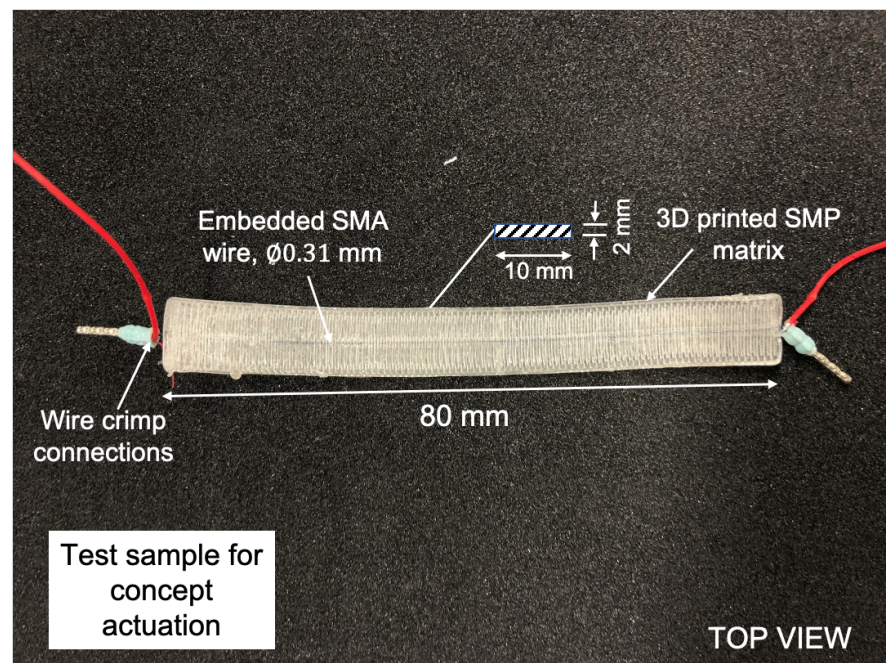


Figure 6. The fabricated SMC with the SMA wire shape set to a 35 mm radius of curvature and prestrained inside the SMP matrix.

2.2. Modelling the Actuator

The design of the SMC actuator was carried out in the commercial FEA software, COMSOL Multiphysics, by simulating time-dependent studies. The applicability of the design workflow was demonstrated in COMSOL by running the actuator's multiphysics interaction and capturing deformations.

2.2.1. Thermomechanical Constitutive Model: Shape Memory Alloy

The Lagoudas [19] thermomechanical sub-routine of the SMA implemented in the Nonlinear Structural Materials Module of COMSOL Multiphysics [23] was utilised for

defining the phenomenological behaviour of the SMA domain. The constitutive model obtained input temperature field T , total stress tensor σ , and additional model parameters to calculate the explicit form of the Gibbs free energy density, $G(\sigma, T, \epsilon_{tr}, \xi)$, to approximate the total strain, ϵ , given by,

$$\epsilon = -\rho \frac{\partial G}{\partial \sigma} = S : \sigma + \epsilon_{th} + \epsilon_{tr} \quad (1)$$

where ϵ_{th} and ϵ_{tr} are the thermal and transformation strain tensor and S is the compliance matrix averaged based on martensitic phase fraction (ξ). The above expression provides the constitutive relation in agreement with the Second Law of Thermodynamics. The model parameters obtained from DSC testing and the literature are provided in Table 2. These parameters were necessary to define the required thermo-mechanical behaviour in COMSOL Multiphysics.

Table 2. Model parameters required for setting up the COMSOL Multiphysics simulation: NiTi SMA [22] parameters with DSC testing data and SMP thermal transport properties [14] with phase transformation parameters from DMA testing data.

Physical Property	Value (units)
Density, ρ	6.45 (g/cm ³)
Martensite start temperature, M_s	66.42 (degC)
Martensite finish temperature, M_f	45.67 (degC)
Austenite start temperature, A_s	56.99 (degC)
Austenite finish temperature, A_f	74.48 (degC)
Stress influence co-efficient, $C_{A,M}$	10 (MPa/degC)
Maximum axial transformation strain, H	0.056
Poisson's ratio, ν_{SMA}	0.33
Young's modulus of austenite, E_A	78 (GPa)
Young's modulus of martensite, E_M	28 (GPa)
Fitting co-efficient of SMP, u	0.1975
Fitting co-efficient of SMP, v	0.234
High temperature of DMA, T_h	119.1 (degC)
Low temperature of DMA, T_l	25.9 (degC)
Glass transition temperature of SMP, T_g	44.59 (degC)
Room temperature, T_r	26 (degC)

2.2.2. Thermomechanical Constitutive Model: Shape Memory Polymer

The constitutive relationship model for the phase transformation behaviour based on the irreversible thermodynamic process provided in Bodaghi et al. [24] is reviewed here. The total strain, ϵ , based on the additive strain assumption is provided as,

$$\epsilon = \zeta_g \epsilon_g + (1 - \zeta_g) \epsilon_r + \alpha (T - T_r) + \epsilon_{in} \quad (2)$$

where α is the thermal expansion co-efficient for thermal strain, ϵ_T , ϵ_{in} is the total inelastic strain, ϵ_r and ϵ_g denote the elastic strains in the corresponding phases, and ζ_g is the volume fraction of the glassy phase in the SMP. The volume fraction of the glassy phase, ζ_g , at a given temperature, T , is represented as trigonometric functions and DMA test fit parameters.

$$\zeta_g = - \frac{\tanh(uT_g - vT) - \tanh(uT_g - vT_h)}{\tanh(uT_g - vT_h) - \tanh(uT_g - vT_l)} \tag{3}$$

where u and v are the DMA test fit parameters, T_h and T_l are the highest and lowest temperatures of the fit data, and T_g is the glass transition temperature of the SMP. The total stress vector, σ , from the Helmholtz free energy density in agreement with the Clausius–Duhem inequality is given as,

$$\sigma = C_e(\epsilon - \alpha(T - T_r) - \epsilon_{in}) \tag{4}$$

where total stiffness, C_e , can be expressed in terms of the compliance matrix, S , as,

$$C_e = (\zeta_g S_g + (1 - \zeta_g) S_r)^{-1} \tag{5}$$

The compliance matrices, S_r and S_g , were calculated from the corresponding Young’s modulus E and Poisson’s ratio ν ,

$$S_r = \begin{pmatrix} \frac{1}{E_r} & \frac{-\nu_r}{E_r} & \frac{-\nu_r}{E_r} & 0 & 0 & 0 \\ \frac{-\nu_r}{E_r} & \frac{1}{E_r} & \frac{-\nu_r}{E_r} & 0 & 0 & 0 \\ \frac{-\nu_r}{E_r} & \frac{-\nu_r}{E_r} & \frac{1}{E_r} & 0 & 0 & 0 \\ 0 & 0 & 0 & \frac{2(1+\nu_r)}{E_r} & 0 & 0 \\ 0 & 0 & 0 & 0 & \frac{2(1+\nu_r)}{E_r} & 0 \\ 0 & 0 & 0 & 0 & 0 & \frac{2(1+\nu_r)}{E_r} \end{pmatrix} \tag{6}$$

The evolution of the inelastic strain in the SMP when the material cools from the rubbery phase to the glassy phase or the recovery of the inelastic strain in the SMP when the material is heated above T_g is given as,

$$\dot{\epsilon}_{in} = \begin{cases} \frac{\dot{\zeta}_g}{\zeta_g} \epsilon_i n, & \text{for } \dot{T} > 0 \\ \dot{\zeta}_g \epsilon_r, & \text{for } \dot{T} < 0 \end{cases} \tag{7}$$

The recovery relation during heating provides current inelastic strain by implicit backward Euler integration as,

$$\epsilon_{in}^t = \frac{\zeta_g^t}{\zeta_g^{t-1}} \epsilon_{in}^{t-1} \tag{8}$$

The evolution relation is then expressed as,

$$\epsilon_{in}^t = (I + \Delta\zeta_g S_r C_e)^{-1} (\epsilon_{in}^{t-1} + \Delta\zeta_g S_r C_e (\epsilon^t - \epsilon_T^t)) \tag{9}$$

where t provides the current time step value, $\Delta\zeta_g = \zeta_g^t - \zeta_g^{t-1}$, and I is the identity matrix. This provides a linear thermo-mechanical constitutive model for the glassy and rubbery phase given as,

$$\sigma = C_{eq}(\epsilon - \epsilon_T - \mu \epsilon_{in}^{t-1}) \tag{10}$$

where,

$$C_{eq} = \begin{cases} C_e, & \mu = \frac{\zeta_g^t}{\zeta_g^{t-1}} \\ C_e (I - \Delta\zeta_g (\Delta\zeta_g I + (S_r C_e)^{-1})^{-1}), & \mu = 1 \end{cases} \tag{11}$$

The first condition of Equation (11) is for heating when $\dot{T} > 0$, and the second condition is for cooling. The mean value of the calibrated parameters for the trigonometric function of ζ_g obtained from fitting DMA test data are provided in Table 2. The modelling parameters were provided as the input in the COMSOL external material subroutine.

2.2.3. Finite Element Model

The geometrically nonlinear multiphysics interaction of the SMC was modelled in COMSOL to study the complex deformation, and acts as a tool to support the design workflow of such complicated systems. The constitutive relationship of the SMP domain needs to be provided as an external stress–strain subroutine to COMSOL, similar to the procedure illustrated in Bodaghi et al. [24].

The user-defined material subroutine was programmed using the C language and compiled as a dynamic link library to be provided as the external material model in COMSOL. The general stress–strain relation socket of the external material module was chosen, as the entire constitutive relations was programmed along with the calculation of the inelastic strain. The socket requires the second Piola–Kirchhoff stress tensor and Jacobian update to be returned as the output in order to solve the structural mechanics problem. The SMP material model was operated in the additive strain approximation, and the SMA material model was forced to be operated in the small strain region for faster convergence. The thermal strain in the SMA and SMP domain was neglected as it would be negligible in comparison with the actuation strain [14].

2.2.4. Validation of the User-Defined Material Model

The accuracy of the user-defined material subroutine was determined by simulating the uniaxial tensile test. The CAD model of the tensile test specimen used for fabrication was imported and defined as the SMP material domain. The portion of tensile test specimen held by the wedges or clamped was neglected from the CAD model. One end of the specimens was applied a fixed constraint simulating the fixed head. The other end was applied a boundary load of 2330.95 N at room temperature and 17.43 N at 70 °C, simulating the final load applied by the moving head. Three observation points were created at the gauge section to extract the extensometer displacement value. A stationary study was set up to extract the true stress and strain values from the simulation. These values were compared with experimental data to determine the accuracy of the external material subroutine.

2.2.5. Validation of the Actuator Model

The SMA wire geometry modelled with a square cross-section having a straight shape was embedded at the centre of the flat SMP geometry. Continuity pairs were created at the interface between the two domains with the assumption of establishing the continuity in strain and temperature without causing delayering. The permanent shape of the SMA wire was provided in the form of initial strain as a function of temperature. Therefore, when A_s was reached, the initial strain ramped up to the shape setting bending strain upon complete transformation at A_f . In order to formulate the model workflow for designing the composite actuator, the multiphysics simulation model was condensed to isothermal assumptions, and complexities were added progressively. The isothermal assumption had the domain temperature interpolated between the set temperature values. During heating, the temperature was linearly increased from room temperature to 100 °C and linearly decreased to room temperature upon cooling. The solid mechanics interface was utilised to input the temperature and define the stress–strain relation of the SMA and SMP. The bending strain for the U-shape-set SMA of a 35 mm radius of curvature was provided by the *Initial Strain* feature of *Shape memory alloy* material module. The simulation study was set up to obtain the displacement of the midpoint over heating and cooling cycles in order to compare with the experimental results. The SMC was modelled as a beam having pin support on one end of the SMA domain and roller support on the other end as the

boundary conditions. COMSOL automatically generates a finer mesh for both the SMA and SMP domains. Figure 7 depicts the overall geometry, mesh, and boundary conditions. This study validated the isothermal domain simulation model with the experimental results and described the trend during the heating and cooling cycles.

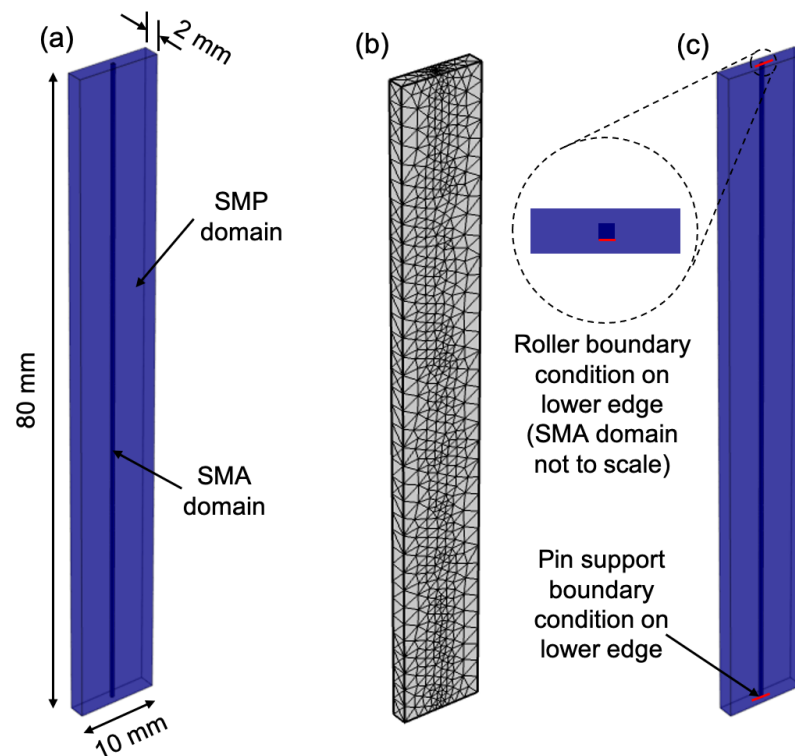


Figure 7. (a) Overall dimension of the COMSOL geometry with the SMA domain modelled as a wire having a square cross-section of $0.31 \text{ mm} \times 0.31 \text{ mm}$, (b) physics-controlled mesh, and (c) roller boundary condition at one end and the pin support boundary condition at other end of the SMA domain.

3. Results and Discussion

3.1. Validation of the User-Defined Material Model

The user-defined SMP material subroutine was validated by simulating the uniaxial tensile test. The stress–strain relation of the simulation data was extracted and compared against the experimental data. Figure 8 shows the good agreement between the simulation and experimental data at room temperature. As the SMP exhibited an elasto-plastic behaviour at room temperature, the strain value was limited close to 1% to demonstrate the behaviour of the actuator in the small strain linear region. Figure 9 shows the good agreement of the trend in the stress with the strain between the simulation and experiment at $70 \text{ }^\circ\text{C}$. It can be seen that the experimental data were noisy due to the high resolution of the load cell and the smaller load difference. The data were linearly fit, and the value of the slope was determined. The offset in the prediction of the stress by the simulation from the experimental data was due to the accumulation of thermal stress in the specimen as it was heated to the set temperature inside the chamber. This offset was taken into account in the simulation model as an external stress value. The result showed that the external SMP material model agreed well with the experimental results.

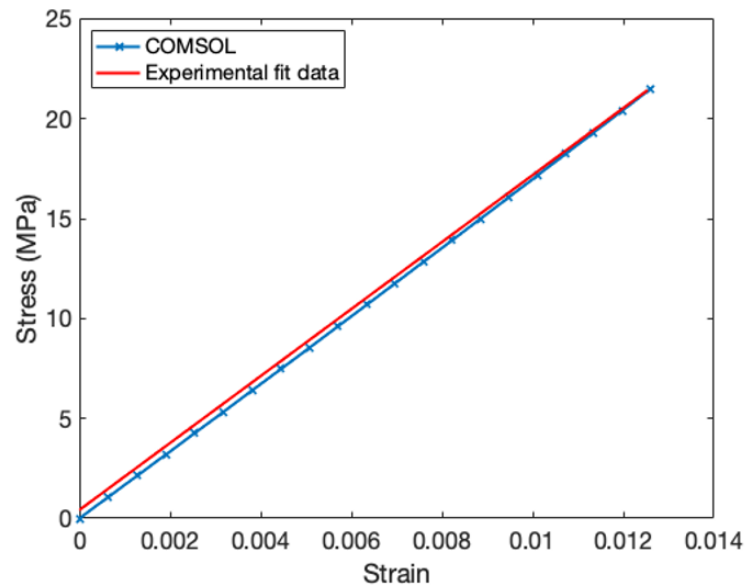


Figure 8. Validation of the SMP material subroutine stress prediction from the simulation (blue colour) with experimental uniaxial tensile test data (red colour) at room temperature with an applied load of 2330.95 N.

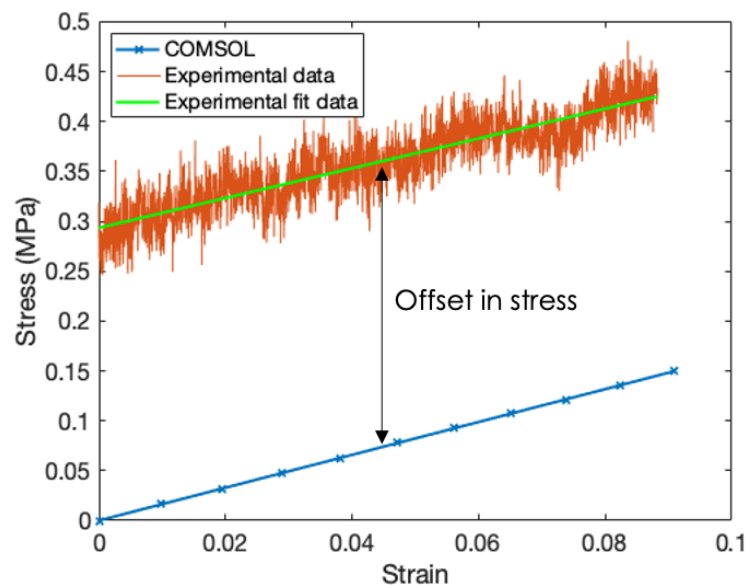


Figure 9. Validation of the SMP material subroutine stress prediction from the simulation (blue colour) with the experimental uniaxial-tensile-test-fit data (green colour) at 70 °C with an applied load of 17.43 N. The offset in stress prediction was caused due to the generation of thermal stress upon heating the test specimen.

3.2. Validation of the Actuator Model

First of all, the bending stiffness of the SMA and SMP domain needed to be roughly estimated in order to interpret the actuation mechanism. Based on the model parameters provided in Table 2, the bending stiffness of the SMA wire could range between 21.54 N mm² ($I = 7.696 \times 10^{-4} \text{ mm}^4$ and $E_M = 28 \text{ GPa}$) in the martensite and 60.02 N mm² ($I = 7.696 \times 10^{-4} \text{ mm}^4$ and $E_A = 78 \text{ GPa}$) in the austenite phase; the bending stiffness of the SMP in the rubbery phase can be 10.981 N mm² ($I = 6.667 \text{ mm}^4$ and $E_r = 1.647 \text{ MPa}$) and in the glassy phase can be 11,114 N mm² ($I = 6.667 \text{ mm}^4$ and $E_g = 1667.1 \text{ MPa}$).

The relative bending stiffness and portion of the SMP softened by the SMA largely influenced the bending or recovery characteristics of the SMC. The experimental setup

had the actuator shown in Figure 6 connected to a 3.3 V DC power supply providing 2.2 A of current. The setup was placed on the ground so that the composite bent upwards when it was actuated. The deflection of the actuator was obtained by post-processing the sequence of images captured by the RGB camera. Figure 10 provides the mid-point deflection of the SMC over time for the experimental specimen and deflection predicted by the simulation model. It is noticeable that the prediction of the simulation model during phase transformation of the SMA matched the trend observed in the experimental values. Although the simulation model predicted the max deflection with an error of 0.8 mm, certain discrepancies were present with the isothermal assumption.

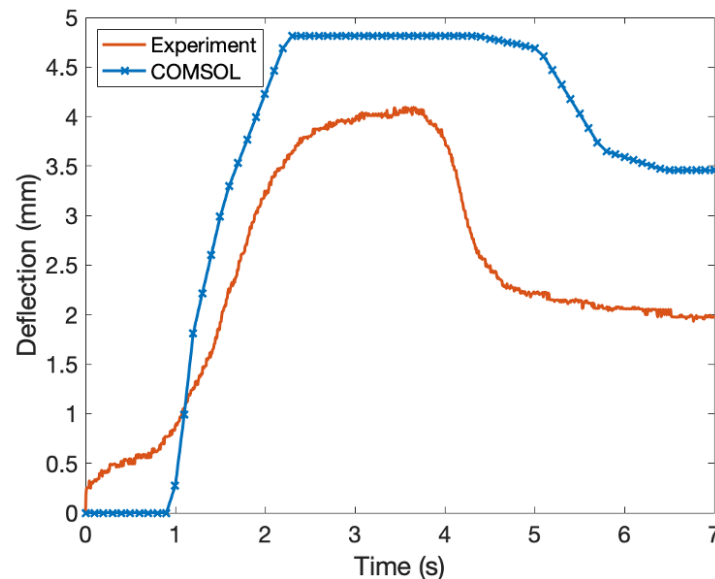


Figure 10. Deflection of the mid-point of the SMC over time obtained from the experiment and COMSOL simulation during heating and cooling cycle for a 2.2 A input current under the isothermal domain assumption.

The simulation model settled at a higher value of deflection as the entire volume fraction of the SMP was softened, whereas the experimental specimen had only a smaller a region of the SMP softened to the rubbery phase due to the low thermal conductivity and variation in the environmental condition. It can also be seen that the SMP was unable to recover its original shape due to the narrow difference in the transformation temperatures and relative stiffness. The chosen SMP material had a glass transition temperature of 44.59 °C, which was closer to the M_f temperature of 45.67 °C. This means that a portion of the SMP would have already transformed to the glassy phase before the SMA became soft in the martensitic phase. This provided the SMP with little time to recover its memorised flat shape. The relative stiffness between the SMA and SMP also affected the shape recovery of the SMP as the bending stiffness of the SMP for the chosen sample in the rubbery phase, 10.981 N mm², was less than that of the bending stiffness of the SMA in the soft martensite phase, 21.54 N mm². Further, the FEA model was exploited to study the viability of the periodic actuation and parametric studies, e.g., increasing the number of SMA wires inside the SMC.

3.3. Periodic Actuation

Figure 11 demonstrates the periodic actuation behaviour of the SMC with one SMA wire. The maximum deflection was obtained in the first cycle, and a decreasing trend was observed for the subsequent actuation cycles. On the contrary, the settled deflection at the end of the cooling for each actuation cycle increased and saturated after four actuation cycles. It can be seen from Figure 11 that the effective amount of actuation decreased for the given geometry. This showed that the actuator was not viable for periodic actuation

after five actuation cycles. The relative stiffness of the rubbery phase SMP and the narrow temperature difference present between T_g and M_f made the actuator inapplicable after five actuation cycles. The sudden decrease in the maximum deflection obtained for the initial actuation cycles was because the prestrain stored in the SMP during the previous cycle was partially recovered before the SMA transformed into austenite. This recovery happened till the SMA wire completely transformed to austenite. The SMA was required to perform additional work to resist the shape recovery due to the stored strain in addition to the stiffness of the rubbery phase SMP. Appropriate geometric dimensions and material parameters are critical in order to achieve periodic actuation. The developed actuator after the sequence of optimisation in the design put together as multiple components can serve as fingers for a robotic gripper end effector. The individual actuator with onboard electronics and control implementation can also be considered as an inchworm robot for navigating complex environments.

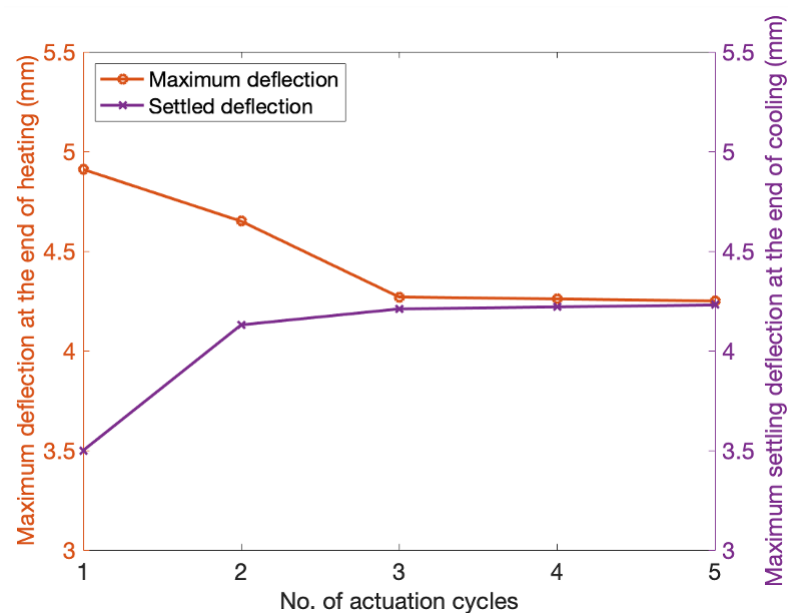


Figure 11. Maximum deflection of the SMC obtained during the heating process (red) and settled deflection of the SMC after the cooling process (purple) obtained for 5 periodic actuation cycles (from the COMSOL simulation).

3.4. Effect of Increasing the Volume Ratio of the SMA Wire

Figure 12 shows the effect of increasing the volume ratio of the SMA wires in the SMC on the maximum and settled deflection at the end of one cycle of actuation. There was a linearly increasing trend in the maximum and recovered deflection. The maximum deflection increased with the addition of another SMA wire because of the combined stiffness of two or more SMA wires in the SMC. The addition of the SMA wires increased the recovery stiffness that needed to be overcome by the soft rubbery phase SMP. Figure 12 shows that the deflection settled at the end of each cooling cycle increased for an increased volume ratio of the SMA. Although providing a solid proof of concept for the use of SMC composite actuators, we expect the tunable performance profile of the actuator to be more fully exploited when co-designed with more complex morphologies.

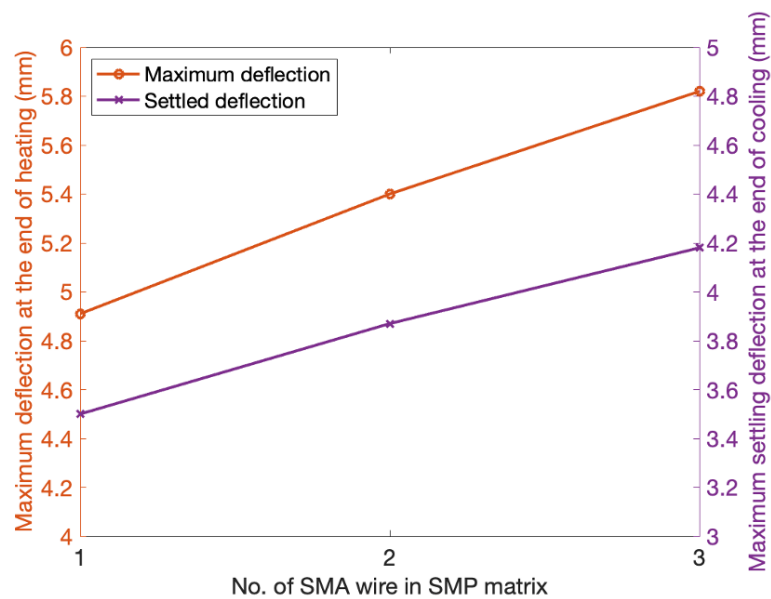


Figure 12. Effect of increasing the volume ratio of the SMA wires in the matrix on the maximum and settled deflection of the SMC at the end of one cycle of actuation (from the COMSOL simulation).

3.5. Reflections from the Experiment

The shape recovery of the SMC was influenced by the difference between the T_g and M_f temperatures. Thus, a numerical study was essential to choose appropriate characterizing temperatures. Although it was essential to have an increased difference in temperature between T_g and M_f , there was an upper limit on the temperature that the SMP could be exposed to before the breakdown of the polymer chains occurred. This is critical while choosing the transformation temperatures of the SMA, as it can save on the energy consumption.

Fabricating the SMC using additive manufacturing techniques and handling thin SMA wire requires care and attention. The SMA wire needs to be slowly deformed along the plane of bending without rotating the wire to achieve appropriate deformation. Care must be employed to not create bumps as it might destroy the subsequent printing layers. It is advisable to have a fixture or jig to be accommodated with the printing bed in order to make this process easier. The adhesion of the SMA with the SMP is important for proper force and heat transfer. Increasing the bed temperature is helpful, but appropriate surface treatment methods are necessary for proper adhesion. The extrusion process of 3D printing causes localised heating of the SMA wire, which can induce phase transformation. This is undesirable as it can damage the composite while printing occurs, thereby discarding the specimen. Therefore, firmly fixing the SMA wire using crimps or a fixture on the printing bed and separate cooling of the wire are helpful.

4. Conclusions

The main objective of this research was to design a bi-state shape memory material composite soft actuator that combined the strengths of the SMA and SMP and provided a tunable performance profile. Experimentation was used to generate a working model in COMSOL Multiphysics, including understanding of the shape memory properties and actuation mechanism, material characterisation, model setup in COMSOL, and proof of concept testing.

The feasibility of the SMC was studied by (i) analysing the shape recovery, (ii) examining the longevity of the periodic actuation, and (iii) evaluating the effect of increasing the number of SMA wires to create a tunable actuating structure. Our results demonstrated the above objectives.

The feasibility of the design was validated through experiments and simulations with COMSOL Multiphysics. The relative stiffness between the SMA and SMP largely influenced the bi-state condition of the SMC. This is important to consider while designing such actuators because a large bending stiffness of the SMA may cause delayering of the specimen and loss in recovery of the shape of the SMP. Furthermore, the viability of the periodic actuator studied through the simulation showed higher deflection during the first cycle of actuation, as there was no stored inelastic strain present in the SMP that needed to be overcome by the SMA. This is critical because in the subsequent actuation cycles, the SMP lost its shape fixity and displayed reduced actuation. Although this served as a limitation on the periodic nature of the SMC, it can be improved by programming the SMP to have lower T_g and the same order of bending stiffness as the SMA wire. The effect of increasing the number of SMA wires in the SMC is considerable and particularly useful for designs requiring a faster heating rate and larger deflection. However, this reduces the robustness of the actuator, as it results in the reduced shape recovery of the SMP.

Additional work can model a more realistic simulation of the real-world operating conditions. Rigorous experimental characterisation testing can be performed to obtain the thermo-mechanical properties of the conductivity for the SMP and the stress influence coefficient of the SMA. Strip or foil SMAs may be able to circumvent the fabrication and heating problems we encountered. Further research holds the experimental and simulation studies for understanding the bistability and evolution of the shape during the thermal cycles of the actuator. This area for exploration will push the boundaries of shape-memory-based soft actuators.

Overall, the complex multiphysics interaction of the SMC presented the necessity for numerical FEA simulation to aid the design of such actuators. The proposed COMSOL Multiphysics workflow can help reduce the wastage of materials, accelerate the process of soft actuator design, and provide a path towards highly optimised composite SMC components.

Author Contributions: Conceptualisation, R.R., A.J.P. and D.H.; methodology, R.R., A.J.P. and D.H.; software, R.R. and D.H.; validation, R.R. and A.J.P.; formal analysis, R.R. and A.J.P.; investigation, R.R., A.J.P. and D.H.; resources, A.J.P. and D.H.; data curation, R.R.; writing—original draft preparation, R.R.; writing—review and editing, A.J.P. and D.H.; visualisation, R.R.; supervision, A.J.P. and D.H.; project administration, A.J.P. and D.H.; funding acquisition, D.H. All authors have read and agreed to the published version of the manuscript.

Funding: This research was funded by CSIRO's Active Integrated Matter Future Science Platform. The APC was funded by CSIRO.

Data Availability Statement: Data is available from <https://research.csiro.au>.

Conflicts of Interest: The authors declare no conflict of interest. The funders had no role in the design of the study; in the collection, analyses, or interpretation of the data; in the writing of the manuscript; nor in the decision to publish the results.

References

1. Huang, W.M.; Song, C.L.; Fu, Y.Q.; Wang, C.C.; Zhao, Y.; Purnawali, H.; Lu, H.B.; Tang, C.; Ding, Z.; Zhang, J.L. Shaping tissue with shape memory materials. *Adv. Drug Deliv. Rev.* **2013**, *65*, 515–535. [[CrossRef](#)] [[PubMed](#)]
2. Huang, Y.; Zhu, M.; Pei, Z.; Xue, Q.; Huang, Y.; Zhi, C. A shape memory supercapacitor and its application in smart energy storage textiles. *J. Mater. Chem. A* **2016**, *4*, 1290–1297. [[CrossRef](#)]
3. Santo, L.; Quadrini, F.; Accettura, A.; Villadei, W. Shape memory composites for self-deployable structures in aerospace applications. *Procedia Eng.* **2014**, *88*, 42–47. [[CrossRef](#)]
4. Coyle, S.; Majidi, C.; LeDuc, P.; Hsia, K.J. Bio-inspired soft robotics: Material selection, actuation, and design. *Extrem. Mech. Lett.* **2018**, *22*, 51–59. [[CrossRef](#)]
5. Grey, A.D.; Rossiter, J. The Next Step—Exponential Life. 2017. Available online: <https://www.bbvaopenmind.com/wp-content/uploads/2017/03/BBVA-OpenMind-book-The-Next-Step-Exponential-Life-1-1.pdf> (accessed on 6 March 2022).
6. Kim, S.; Laschi, C.; Trimmer, B. Soft robotics: A bioinspired evolution in robotics. *Trends Biotechnol.* **2013**, *31*, 287–294. [[CrossRef](#)] [[PubMed](#)]
7. Majidi, C. Soft-Matter Engineering for Soft Robotics. *Adv. Mater. Technol.* **2019**, *4*, 1800477. [[CrossRef](#)]

8. Manzo, J.; Garcia, E. Evolutionary flight and enabling smart actuator devices. In *Active and Passive Smart Structures and Integrated Systems 2007*; International Society for Optics and Photonics: Bellingham, WA, USA, 2007; Volume 6525, pp. 163–170.
9. Tobushi, H.; Hayashi, S.; Sugimoto, Y. Two-way bending properties of shape memory composite with SMA and SMP. *Materials* **2009**, *2*, 1180–1192. [[CrossRef](#)]
10. Li, Z.; Huang, R.; Liu, Z. A Periodic Deformation Mechanism of a Soft Actuator for Crawling and Grasping. *Adv. Mater. Technol.* **2019**, *4*, 1–10. [[CrossRef](#)]
11. Kang, M.; Pyo, Y.; Jang, Y.J.; Park, Y.; Son, Y.H.; Choi, M.; Ha, J.W.; Chang, Y.W.; Lee, C.S. Design of a shape memory composite (SMC) using 4D printing technology. *Sens. Actuators A Phys.* **2018**, *283*, 187–195. [[CrossRef](#)]
12. Pretsch, T. Review on the functional determinants and durability of shape memory polymers. *Polymers* **2010**, *2*, 120–158. [[CrossRef](#)]
13. Song, J.J.; Chen, Q.; Naguib, H.E. Constitutive modelling and experimental validation of the thermo-mechanical response of a shape memory composite containing shape memory alloy fibers and shape memory polymer matrix. *J. Intell. Mater. Syst. Struct.* **2016**, *27*, 625–641. [[CrossRef](#)]
14. Saunders, R.; Hartl, D.; Malak, R.; Lagoudas, D. Design and analysis of a self-folding SMA-SMP composite laminate. In Proceedings of the International Design Engineering Technical Conferences and Computers and Information in Engineering Conference, Buffalo, NY, USA, 17–20 August 2014.
15. Bovesecchi, G.; Corasaniti, S.; Costanza, G.; Piferi, F.P.; Tata, M.E. Deployment of solar sails by joule effect: Thermal analysis and experimental results. *Aerospace* **2020**, *7*, 180. [[CrossRef](#)]
16. Taya, M.; Liang, Y.; Namli, O.C.; Tamagawa, H.; Howie, T. Design of two-way reversible bending actuator based on a shape memory alloy/shape memory polymer composite. *Smart Mater. Struct.* **2013**, *22*, 105003. [[CrossRef](#)]
17. Ghosh, P.; Rao, A.; Srinivasa, A.R. Design of multi-state and smart-bias components using shape memory alloy and shape memory polymer composites. *Mater. Des.* **2013**, *44*, 164–171. [[CrossRef](#)]
18. COMSOL—Software for Multiphysics Simulation. Available online: <https://www.comsol.com/> (accessed on 6 March 2022).
19. Lagoudas, D.C. *Shape Memory Alloys: Modelling and Engineering Applications*; Springer: Berlin/Heidelberg, Germany, 2008.
20. Hu, G.; Damanpack, A.; Bodaghi, M.; Liao, W. Increasing dimension of structures by 4D printing shape memory polymers via fused deposition modelling. *Smart Mater. Struct.* **2017**, *26*, 125023. [[CrossRef](#)]
21. Standard, A. *D638: Standard Test Method for Tensile Properties of Plastics*; ASTM International: West Conshohocken, PA, USA, 2010.
22. Cianchetti, M. Fundamentals on the use of shape memory alloys in soft robotics. In *Interdisciplinary Mechatronics*; Habib, M.K., Davim, J.P., Eds.; Wiley Online Library: Hoboken, NJ, USA, 2013.
23. Nonlinear Structural Material Analysis Software from COMSOL. Available online: <https://www.comsol.com/nonlinear-structural-materials-module> (accessed on 6 March 2022).
24. Feng, Y.; Bodaghi, M.; Liao, W. Numerical/experimental assessment of 3D-printed shape-memory polymeric beams. *J. Appl. Polym. Sci.* **2019**, *136*, 47422. [[CrossRef](#)]